ISSN 1726-5479

SENSORS & TRANSDUCERS

3 vol. 14-1 Special /12

Physical and Chemical Sensors & Wireless Sensor Networks

International Frequency Sensor Association Publishing

IFSA

Sensors & Transducers

Volume 14-1, Special Issue
March 2012

www.sensorsportal.com

ISSN 1726-5479

Sensors & Transducers Journal (ISSN 1726-5479) is a peer review international journal published monthly online by International Frequency Sensor Association (IFSA).
Available in electronic and on CD.

Sensors & Transducers Journal

Contents

Volume 14-1
Special Issue
March 2012

www.sensorsportal.com

ISSN 1726-5479

Research Articles

Physical and Chemical Sensors & Wireless Sensor Networks (Foreword)
Sergey Y. Yurish, Petre Dini I

From Smart to Intelligent Sensors: A Case Study
Vincenzo Di Lecce, Marco Calabrese 1

Smart Optoelectronic Sensors and Intelligent Sensor Systems
Sergey Y. Yurish 18

Accelerometer and Magnetometer Based Gyroscope Emulation on Smart Sensor for a Virtual Reality Application
Baptiste Delporte, Laurent Perroton, Thierry Grandpierre and Jacques Trichet 32

Top-Level Simulation of a Smart-Bolometer Using VHDL Modeling
Matthieu Denoual and Patrick Attia 48

A Novel Liquid Level Sensor Design Using Laser Optics Technology
Mehmet Emre Erdem and Doğan Güneş 65

Recognition of Simple Gestures Using a PIR Sensor Array
Piotr Wojtczuk, Alistair Armitage, T. David Binnie, Tim Chamberlain 83

Sinusoidal Calibration of Force Transducers Using Electrodynamic Shaker Systems
Christian Schlegel, Gabriela Kiekenap, Bernd Glöckner, Rolf Kumme 95

Experimental Validation of a Sensor Monitoring Ice Formation over a Road Surface
Amedeo Troiano, Eros Pasero, Luca Mesin 112

Acoustic Emission Sensing of Structures under Stretch
Irinela Chilibon, Marian Mogildea, George Mogildea 122

Differential Search Coils Based Magnetometers: Conditioning, Magnetic Sensitivity, Spatial Resolution
Timofeeva Maria, Allegre Gilles, Robbes Didier, Flament Stéphane 134

Silicon Photomultipliers: Dark Current and its Statistical Spread
Roberto Pagano, Sebania Libertino, Giusy Valvo, Alfio Russo, Delfo Nunzio Sanfilippo, Giovanni Condorelli, Clarice Di Martino, Beatrice Carbone, Giorgio Fallica and Salvatore Lombardo 151

An Integrated Multimodal Sensor for the On-site Monitoring of the Water Content and Nutrient Concentration of SoilbyMeasuring the Phase and Electrical Conductivity
Masato Futagawa, Md. Iqramul Hussain, Keita Kamado, Fumihiro Dasai, Makoto Ishida, Kazuaki Sawada 160

Design and Evaluation of Impedance Based Sensors for Micro-condensation Measurement under Field and Climate Chamber Conditions
Geert Brokmann, Michael Hintz, Barbara March and Arndt Steinke 174

A Parallel Sensing Technique for Automatic Bilayer Lipid Membrane Arrays Monitoring
Michele Rossi, Federico Thei and Marco Tartagni 185

Development of Acoustic Devices Functionalized with Cobalt Corroles or Metalloporphyrines for the Detection of Carbon Monoxide at Low Concentration
Meddy Vanotti, Virginie Blondeau-Patissier, David Rabus, Jean-Yves Rauch, Jean-Michel Barbe, Sylvain Ballandras 197

Group IV Materials for High Performance Methane Sensing in Novel Slot Optical Waveguides at 2.883 μm and 3.39 μm
Vittorio M. N. Passaro, Benedetto Troia and Francesco De Leonardis 212

The Impact of High Dielectric Permittivity on SOI Double-Gate Mosfet Using Nextnano Simulator
Samia Slimani, Bouaza Djellouli 231

A Novel Sensor for VOCs Using Nanostructured ZnO and MEMS Technologies
H. J. Pandya, Sudhir Chandra and A. L. Vyas 244

$La_{0.7}Sr_{0.3}MnO_3$ Thin Films for Magnetic and Temperature Sensors at Room Temperature
Sheng Wu, Dalal Fadil, Shuang Liu, Ammar Aryan, Benoit Renault, Jean-Marc Routoure, Bruno Guillet, Stéphane Flament, Pierre Langlois and Laurence Méchin 253

Cell-Culture Real Time Monitoring Based on Bio-Impedance Measurements
Paula Daza, Daniel Cañete, Alberto Olmo, Juan A. García and Alberto Yúfera 266

Authors are encouraged to submit article in MS Word (doc) and Acrobat (pdf) formats by e-mail: editor@sensorsportal.com
Please visit journal's webpage with preparation instructions: http://www.sensorsportal.com/HTML/DIGEST/Submition.htm

International Frequency Sensor Association (IFSA).

The 3rd International Conference on Sensor Device Technologies and Applications

SENSORDEVICES 2012

19 - 24 August 2012 - Rome, Italy

Deadline for papers: 5 April 2012

Tracks: Sensor devices - Ultrasonic and Piezosensors - Photonics - Infrared - Geosensors - Sensor device technologies - Sensors signal conditioning and interfacing circuits - Medical devices and sensors applications - Sensors domain-oriented devices, technologies, and applications - Sensor-based localization and tracking technologies

http://www.iaria.org/conferences2012/SENSORDEVICES12.html

The 6th International Conference on Sensor Technologies and Applications

SENSORCOMM 2012

19 - 24 August 2012 - Rome, Italy

Deadline for papers: 5 April 2012

Tracks: Architectures, protocols and algorithms of sensor networks - Energy, management and control of sensor networks - Resource allocation, services, QoS and fault tolerance in sensor networks - Performance, simulation and modelling of sensor networks - Security and monitoring of sensor networks - Sensor circuits and sensor devices - Radio issues in wireless sensor networks - Software, applications and programming of sensor networks - Data allocation and information in sensor networks - Deployments and implementations of sensor networks - Under water sensors and systems - Energy optimization in wireless sensor networks

http://www.iaria.org/conferences2012/SENSORCOMM12.html

The 5th International Conference on Advances in Circuits, Electronics and Micro-electronics

CENICS 2012

19 - 24 August 2012 - Rome, Italy

Deadline for papers: 5 April 2012

Tracks: Semiconductors and applications - Design, models and languages - Signal processing circuits - Arithmetic computational circuits - Microelectronics - Electronics technologies - Special circuits - Consumer electronics - Application-oriented electronics

http://www.iaria.org/conferences2012/CENICS12.html

Sensors & Transducers Journal, Vol. 14-1, Special Issue, March 2012, pp. 212-230

www.sensorsportal.com

Sensors & Transducers

ISSN 1726-5479

http://www.sensorsportal.com

Group IV Materials for High Performance Methane Sensing in Novel Slot Optical Waveguides at 2.883 µm and 3.39 µm

[1] Vittorio M. N. PASSARO, [2] Benedetto TROIA and [1] Francesco DE LEONARDIS

[1] Photonics Research Group, Dipartimento di Elettrotecnica ed Elettronica, Politecnico di Bari
Via Edoardo Orabona n. 4, 70125 Bari, Italy

[2] Photonics Research Group and CNIT UdR Bari, Dipartimento di Elettrotecnica ed Elettronica, Politecnico di Bari, Via Edoardo Orabona n. 4, 70125 Bari, Italy
E-mail: passaro@deemail.poliba.it

Received: 9 November 2011 /Accepted: 20 December 2011 /Published: 12 March 2012

Abstract: In this paper a detailed investigation of novel photonic sensors based on slot waveguides has been carried out. Appropriate alloys of group IV materials, such as germanium (Ge), silicon (Si), carbon (C) and tin (Sn), are applied in silicon-on-insulator (SOI) technology for homogeneous optical sensing at 2.883 µm and 3.39 µm. Electronic and optical properties of group IV alloys have been investigated. In addition, we have designed novel group IV vertical slot waveguides in order to achieve ultra-high sensitivities, as well as good fabrication tolerances. All these features have been compared with well-known SOI slot waveguides for optical label-free homogeneous sensing at 1.55 µm. In conclusion, theoretical investigation of ring resonators based on these novel slot waveguides has revealed very good results in terms of ultra high sensing performance of methane gas, i.e., limit of detection ~ 3.6×10^{-5} RIU and wavelength sensitivity > 2×10^{3} nm/RIU. *Copyright © 2012 IFSA.*

Keywords: Slot waveguide, Mid-IR gas sensing, Ring resonator, Group IV photonics.

1. Introduction

Photonic label-free sensors for homogeneous optical sensing have been investigated and fabricated in the last decade because of their high performance, in particular high sensitivity (*S*) and ultra-low limit of detection (LOD) [1]. Nowadays, a novel field of application, i.e. mid-IR gas optical sensing, is investigating. Reasons that encourage this novel field of interest are mainly related to environmental monitoring, for example attention to harmful gases like carbon dioxide (CO_2), carbon monoxide (CO), methane (CH_4) and sulfur dioxide (SO_2), to name a few [2-3]. In addition, all previous gases are

characterized by absorption spectra in near mid-IR, especially in the range 2-8 μm. Then, ingenious techniques are needed to extend group IV Photonics from near-IR to mid-IR wavelength range [4-5].

In this paper, novel group IV vertical slot waveguides are investigated at two mid-IR wavelengths, 2.883 μm and 3.39 μm, by using full-vectorial 2D Finite Element Method (FEM) [6]. We have analyzed the influence of slot waveguide geometrical parameters (slot gap region, height and width of slot wires) and their optimization, in order to improve the field confinement in the slot region, thus the sensing performance in terms of homogeneous sensitivity (S_h) and limit of detection (LOD). A novel approach is developed to achieve the best alloys of group IV materials enabling ultra-high sensing at mid-IR wavelengths.

It is known that the integration of high performance slot waveguides in resonant architectures such as ring resonators, micro-disks and racetrack resonators, allows to achieve ultra low LODs and high wavelength sensitivities for chemical and biochemical sensing (e.g., glucose detection, DNA sequencing by hybridization, early tumor diagnosis in biomedical applications, gas sensing, and so on).

Moreover, the CMOS-compatible technology can ensure photonic sensor mass-scale production enhancing, at the same time, the photonic biochemical sensor performances, particularly in the areas of light-analyte interaction, device miniaturization and multiplexing, and fluidic design and integration. In this context, optical Lab-on-a-chip systems based on photonic biochemical sensors represent the state of the art of photonic sensing.

2. Theoretical Investigation of Slot Waveguide Structures

Slot waveguides represent a very interesting and promising architecture for photonic chemical and bio-chemical sensing. In fact, it is possible to confine an extremely high optical field in a low refractive index (RI) region, well known as a slot region. Its physical and theoretical investigation enables to understand how this feature is characterized and which are the most important parameters involved in this phenomena. In Fig. 1, schematic top and cross-sectional views of a typical slot waveguide are sketched. In particular, the structure consists of a thin low-index (n_L) slot embedded between two high-index (n_H) regions (wires).

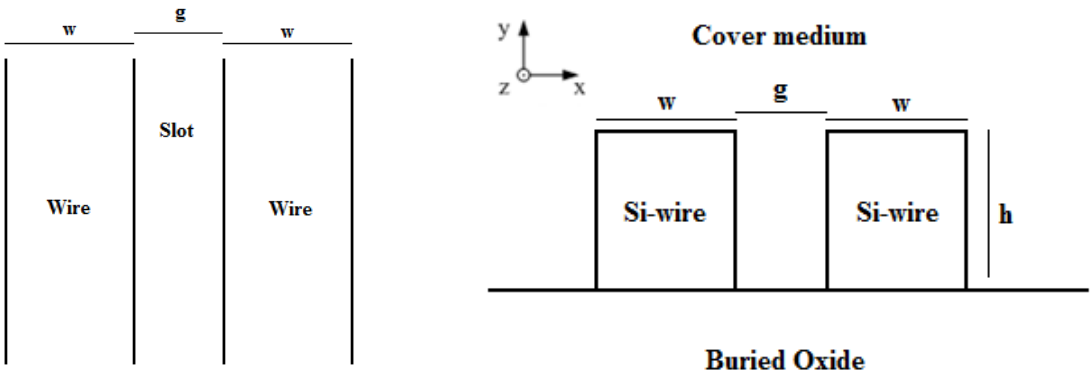

Fig. 1. Top (left) and cross-sectional (right) views of a standard SOI single-slot waveguide.

Due to the large index contrast at the interfaces, the normal electric field (*E*-field) undergoes a large discontinuity, which results in a field enhancement in the low-index region [7]. In fact, in Eq. (1) E_L is the *E*-field in the slot region, while E_H is the *E*-field in high index regions (Si-wires):

$$|E_L| = \left(\frac{n_H}{n_L}\right)^2 |E_H| \tag{1}$$

Thus, the larger the refractive index contrast ($\Delta n = n_H - n_L$) between slot region and Si-wires, the stronger the field confinement in the slot area. A SOI vertical slot waveguide, characterized by geometrical parameters w = 180 nm, h = 324 nm, g = 70 nm, and simulated at λ = 1550 nm (n_{Si} = 3.45, n_{SiO2} = 1.45, n_{air} = 1), can exhibit a very high field confinement in the slot region, due to the high refractive index contrast (Δn = 2) of the structure, as shown in Fig. 2.

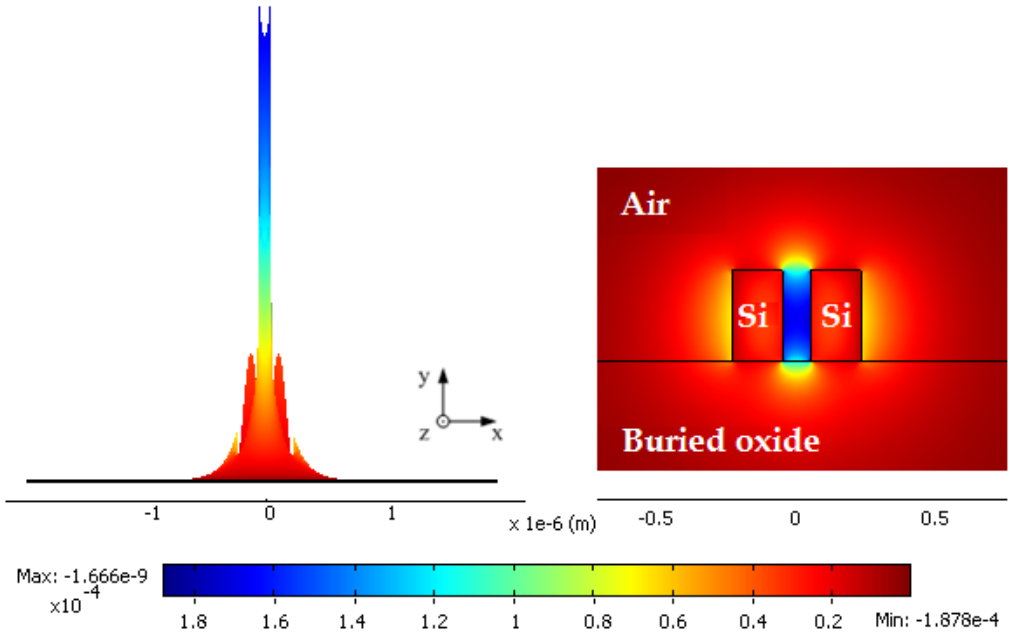

Fig. 2. E_x-field intensity and spatial distribution of the TE-polarized slot mode in SOI.

In vertical slot waveguides, the principal electrical field component undergone discontinuities is the E_x-field one, simply because x-direction is the only one subjected to refractive index change in the optical confinement area. For this reason, the investigated fundamental eigenmode is TE-polarized.

In this paper, the most important parameters taken into account for optimization and design of novel group IV-based SOI slot waveguides, are field confinements in different regions of interest (cover and slot), as well as sensitivity for homogeneous sensing. In particular, optical power confinement factor can be defined as the fraction of total power, confined and guided in the region of interest, i.e. in the cover medium Γ_c and in the slot region Γ_s, as follows:

$$\Gamma_C = \frac{\iint\limits_C \left|\vec{E}(x,y)\right|^2 dxdy}{\iint\limits_\infty \left|\vec{E}(x,y)\right|^2 dxdy} \tag{2}$$

$$\Gamma_S = \frac{\iint\limits_S \left|\vec{E}(x,y)\right|^2 dxdy}{\iint\limits_\infty \left|\vec{E}(x,y)\right|^2 dxdy} \tag{3}$$

In Eq. (2) and (3), the integrals are calculated inside the regions of interest (cover *C*, and slot *S*). In case of homogeneous sensing, when the effective index change is produced by a change of cover medium refractive index, the sensitivity S_h is defined by the following expression [8]:

$$S_h = \left.\frac{\partial n_{eff}}{\partial n_c}\right|_{n_c=n_c^0} = \frac{2\cdot n_c^0}{\eta_0 \cdot P}\iint_C \left|\vec{E}(x,y)\right|^2 dxdy = \frac{2\cdot n_c^0 \cdot \Gamma_c}{\eta_0 \cdot P}\iint_\infty \left|\vec{E}(x,y)\right|^2 dxdy$$
$$P = \iint_\infty \left[\left(\vec{E}\times\vec{H}^* + \vec{E}^*\times\vec{H}\right)\cdot\hat{z}\right]dxdy\,, \tag{4}$$

where n_{eff} is the propagating mode effective index, n_c is the cover medium RI, n_c^0 is the unperturbed value of n_c, η_0 is the free space impedance (377 Ω), z is the unit vector of the propagation direction, and $\vec{E},\vec{H}$ are the electric and magnetic field vectors, respectively. From Eq. (4), it is evident that the waveguide sensitivity S_h linearly depends on the optical field confinement factor in the cover medium (Γ_c). By this way, the practical approach used for the optimization consists in obtaining the maximum E_x-field confinement in the cover medium, in particular in the slot region (Γ_s), which is a sub-domain of the whole integration domain selected in Eq. (2). The rigorous numerical approach based on 2D full-vectorial FEM has been applied in order to find the optical properties of each structure in terms of n_{eff}, Γ_c , Γ_s, and S_h.

2.1. Sensing Principles

In general, chemical and biochemical integrated photonic sensors are based on three fundamental physical sensing principles: homogeneous sensing, surface sensing and optical absorption. The first one has been already considered in the previous paragraph and it will be used in this paper for design purposes. In fact, by assuming that the slot waveguide (see Fig. 2) is initially exposed to air (n_{air} = 1 @ λ = 1.55 μm), when a specific gas (e.g., He, CO_2, Ar, N_2, C_2H_2) will cover the sensor surface, a cover refractive index change Δn_c will be caused (e.g., n_{N2} = 1.000294 @ λ = 1.55 μm, thus a cover refractive index change $\Delta n_c = n_{N2} - n_{air}$ = 0.0294 % is induced), producing a small effective index change Δn_{eff} of the guided optical mode, which can be measured by an appropriate readout approach [9].

In surface sensing, a change of modal effective index n_{eff} of the propagating optical signal is due to a change of thickness of an ultra-thin layer of selective receptor molecules, which are immobilized on the functionalized waveguide surface, as sketched in Fig. 3.

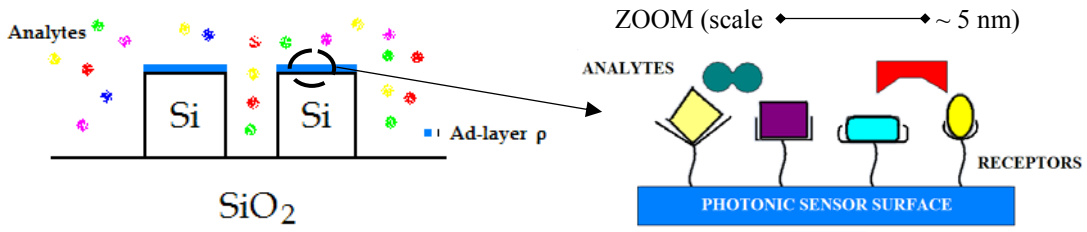

Fig. 3. Schematic representation of surface sensing in a typical SOI slot waveguide.

Thus, if the thickness of the sensor surface layer is initially set to ρ_0 before exposing to the chemical sample, the final thickness ρ will be $\rho_0 + \rho_1$ after the selective adsorption, being ρ_1 the ad-layer thickness. This thickness change $\Delta\rho$ will induce an effective index change Δn_{eff} , so defining a surface sensitivity as:

$$S_S = \frac{\partial n_{eff}}{\partial \rho}, \text{ where } \Delta n_{eff} = \frac{n_m^2 - \left(n_C^0\right)^2}{\eta_0 P} \iint_M \left|\vec{E}(x,y)\right|^2 dxdy \quad (5)$$

In Eq. (5), n_m is the molecular ad-layer refractive index and M is the region in which the ad-layer increases. Optimized slot waveguides, working at λ = 1550 nm, can exhibit a surface sensitivity better than 10^{-4} nm^{-1} [8].

Both homogeneous and surface sensing identify a photonic sensor type called "refractive index sensor", because the transduction process consists in a modal effective index change in both principles. On the contrary, the last sensing principle based on optical absorption involves the measurement of the propagating mode optical intensity, instead of its effective index. The absorption coefficient α (cm^{-1}) depends on the operative wavelength of the photonic signal and on analyte (e.g., gas, solid, liquid solutions) electronic and optical properties. By this way, it is possible to detect gas species or chemical analytes with high sensitivity and selectivity, by simply analyzing the transmission spectra of the light intensity in a suitable wavelength range. In particular, the photonic signal intensity is related to the gas or analyte concentration via the Lambert-Beer law:

$$I = I_0 \exp(-\alpha L); \quad \alpha = \varepsilon C, \quad (6)$$

where I is the light intensity at the end section of the interaction path length L, I_0 is the light intensity at the initial section of the device sensible area, ε is the molar absorptivity and C is the concentration of absorbing species in the solution. Then, it is possible to register steep peaks in the transmission spectra corresponding to specific operative wavelengths, properly selected among the absorption wavelengths of species to be detected, as shown in Fig. 4 in case of some gases. Integrated photonic sensors based on optical absorption exhibit ultra low LOD, of the order of pg/mm^2 or ng/mL.

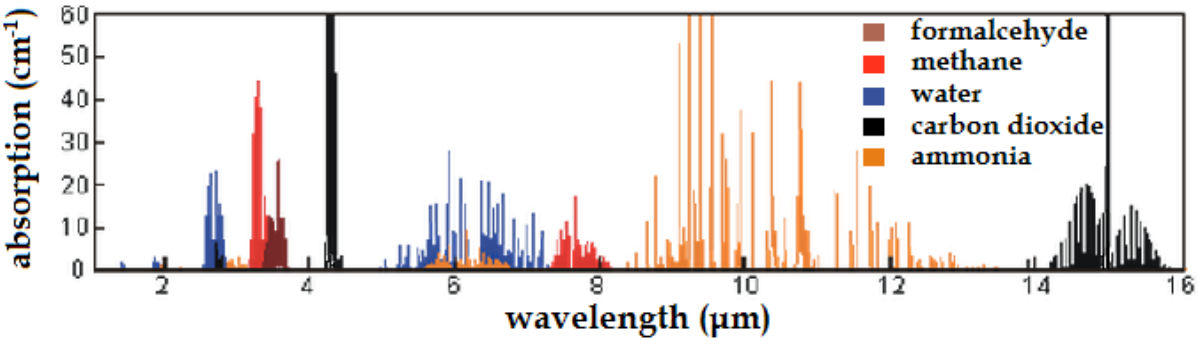

Fig. 4. Absorption spectra of harmful gases and chemical substances in mid-IR.

3. Novel SOI Slot Waveguides Based on Group IV Materials and Compounds

In this section, different combinations of group IV materials, i.e. germanium (Ge), silicon (Si), carbon (C) and tin (Sn), are presented to form slot optical waveguides, as sketched in Fig. 5 [10].

FEM approach has been used for the optical analysis of these structures. In FEM mesh generation for effective index and modal profile calculation, triangular vector-elements have been adopted with at least 30,000 elements. In particular, the whole domain region has a total area of 9 μm^2 (4 × 2.25 μm^2). Changing the boundary condition from a perfect electric to a perfect magnetic conductor, only a

negligible influence on results occurs. In all simulations, the buried oxide layer is assumed very thick, 1 μm that is why the silicon substrate is not shown in Fig. 5.

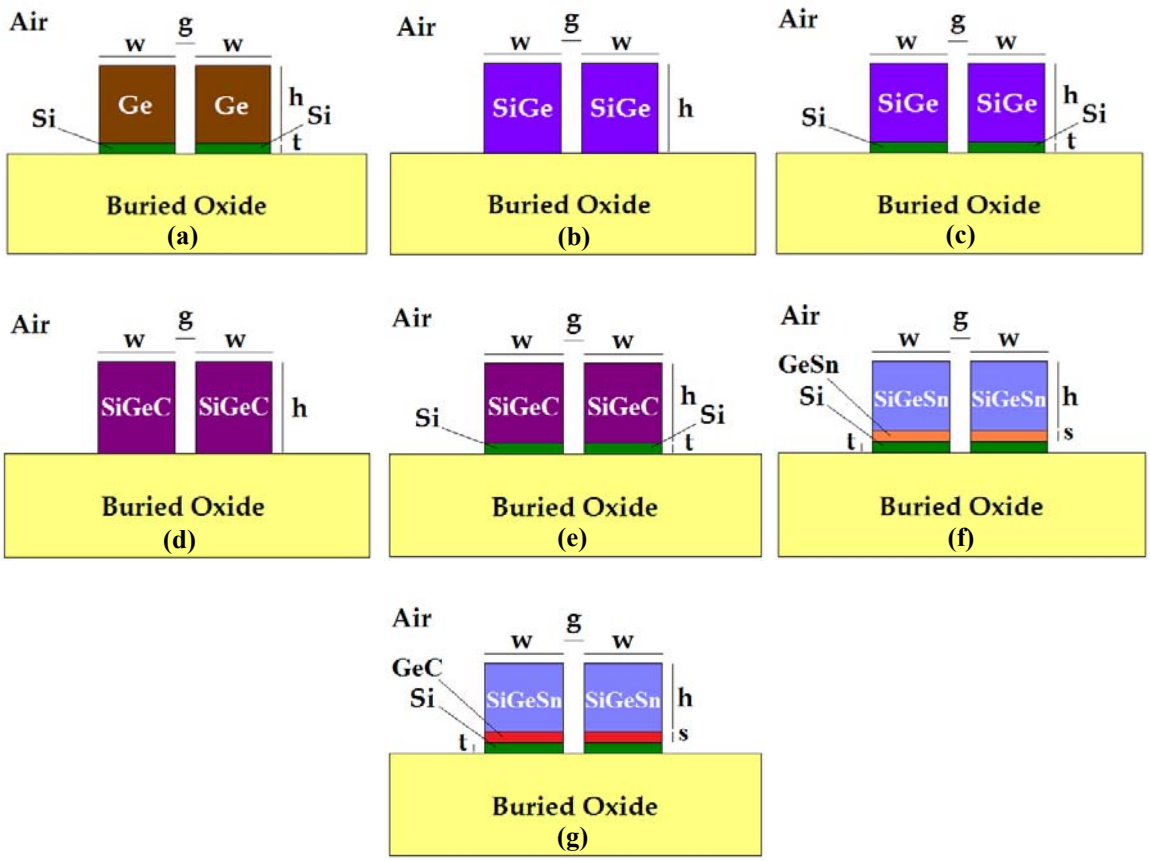

Fig. 5. SOI slot waveguides based on different combinations of group IV materials and alloys.

The first step of the study and optimization of these novel slot waveguides consists in the material optical and electronic characterization. To this purpose, refractive indices of Si, Ge, C, Sn and SiO_2, have been calculated by considering Sellmeier dispersion equations [11-13]. Consequently, linear interpolation has been implemented in order to estimate the optical properties of all alloys shown in Fig. 5 at both mid-IR wavelengths, λ = 2.883 μm and λ = 3.39 μm [14]. In particular, linear interpolation has been applied to derive refractive indices of group IV alloys from those of each single element, each one weighted by the corresponding percentage with which it compares in the specific alloy, i.e., $n_{YZ} = n_Y x + n_Z(1-x)$ for each Y_xZ_{1-x} compound. All numerical results calculated by the theoretical model are listed in Table 1.

At mid-IR wavelengths, it is very important to analyze and ensure very low propagation losses. In fact, the longer the wavelength the greater the spatial distribution of the *E*-field in the guided region. In this way, it is clear that a percentage of the total confined optical field, will interact and distribute into the buried oxide layer. A lot of investigations have been carried out in order to measure and predict propagation losses of different well-known technologies [15]. In particular, using linear interpolation and assuming that a significant fraction (30 %) of the guided-mode power is confined in the buried insulator layer, the estimated wavelength range is from 1.2 μm to 3.6 μm for silicon-on-insulator (SOI) configuration with propagation losses less than 1 dB/cm. On the other hand, the very high value of absorption coefficient into the buried silicon oxide layer could compromise the behavior of the guided-wave photonic sensors. As it is know, the absorption coefficient for the bulk silicon oxide presents a

spike in the wavelength range 2.6-2.8 μm. Consequently, 2.883 μm represents the limit wavelength at which buried oxide exhibits propagation losses higher than 1 dB/cm, but still acceptable for μm-size integrated lab-on-chip (~ 2 dB/cm). Moreover, strain-balanced Ge_zSn_{1-z}-$Si_xGe_ySn_{1-x-y}$ multiple-quantum-well lasers are available now at the operative wavelength of 2.883 μm [16]. Obviously, it is necessary to confine a high percentage of E_x-field in the slot region in order to prevent high propagation losses.

Table 1. Refractive indices of group IV materials and alloys @ 2.883 μm and @ 3.39 μm.

Compounds	RI @ 2.883 μm	RI @ 3.39 μm
Ge	4.048	4.035
Si	3.434	3.429
SiO_2	1.502	1.488
$Si_{0.15}Ge_{0.85}$	3.956	3.944
$Si_{0.08}Ge_{0.91}C_{0.01}$	3.982	3.970
$Si_{0.08}Ge_{0.78}Sn_{0.14}$	4.320	4.296
$Ge_{0.97}C_{0.03}$	3.998	3.985
$Ge_{0.91}Sn_{0.09}$	4.255	4.234

Thus, for an operation wavelength of about 2.883 μm, it becomes crucial to hold the propagation losses less than 2 dB/cm in order to realize μm-size integrated lab-on-chip systems. In this sense, it is essential to guarantee two different conditions: i) the material system proposed must have very low propagation losses in the mid-IR region; ii) the fraction of guided-mode power in the buried insulator layer must be significantly low. For what concerning the first condition, each material system configuration proposed by us exhibits specific optimized infrared wavelength ranges of operation. For example, the Ge-on-Si material configuration is characterized by the operative range 1.9-16.8 μm and 140-200 μm at 300 K, where the fundamental mode propagation loss is less than 2 dB/cm. Analogously, the material systems SiGe and SiGe-on-Si, shown in Fig. 5 (b)-(c), respectively, exhibit both operative wavelength ranges, 1.6-12 μm and 100-200 μm. In addition, material systems based on GeSn alloy and GeSn-on-Si configuration, as in Fig. 5 (f)-(g), exhibit low propagation losses (< 2 dB/cm) in the range 2.2-19 μm, as well as the alloy SiGeC and the material system SiGeC-on-Si. Therefore, the limiting factor is represented by the losses into the SiO_2 buried layer. To give an estimation of losses, it is useful the following relationship [15]:

$$\alpha_{loss}^{(prop)} = \Gamma_{HI}\alpha_{HI}^{(bulk)} + \Gamma_{SiO_2}\alpha_{SiO_2}^{(bulk)}, \tag{7}$$

where $\Gamma_{HI}, \Gamma_{SiO_2}$ are the optical power fractions in high index (HI) material and silicon oxide layer, respectively, and $\alpha_{HI}^{(bulk)}, \alpha_{SiO_2}^{(bulk)}$ are the relative bulk optical losses. Thus, the total losses could be controlled by reducing the fraction of the guided-mode power in the buried insulator, as lower than 30%. In fact, in optimized slot waveguides the optical mode propagates in air (slot region), as previously shown in Fig. 2.

Finally, last considerations concern with the definition of compositional spaces selected for material systems and alloys. As shown in Table 1, each group IV alloy is characterized by a compositional space identified by a precise set of material titles. The design criteria selected for the optical and electronic characterization consists in imposing a high refractive index of slot wires in order to maximize the E_x-Field confinement in the slot region, as given in Eq. (1). In addition, bandgap engineering allows to set the electronic bandgap of alloys higher than the photon energy (E_p) at both mid-IR operative wavelengths (E_p= 0.4304 eV @ 2.883 μm, E_p= 0.366 eV @ 3.39 μm), assuring

structure optical transparency [14]. Thus, it is possible to prevent absorption losses, according to above explained requirements and aspects.

3.1. Slot Waveguide Optimization and Performance

Slot waveguides are characterized by a number of geometrical parameters, i.e. wire width *w*, silicon thickness *t* and alloy layer thicknesses indicated with *s*, and *h*, and slot region gap *g*, as sketched in Fig. 5. In particular, the whole wire height is $H = t + s + h$. All these parameters define a geometrical multi-dimensional space that can be generally identified by the following expression:

$$\langle h, g, t, w, s \rangle \tag{8}$$

The optimization process consists in calculating the unique geometrical configuration that allows to achieve the best performances (S_{h_MAX}, Γ_{c_MAX}, Γ_{s_MAX}), for a given slot waveguide. The method consists in an iterative procedure. In particular, several steps are needed by changing one dimension of the geometrical space of Eq. (8), one at one time, and simultaneously fixing all other ones during the same iteration. This iterative method enables to set the optimized waveguide geometrical architecture and it is used for each optimization procedure presented in this paper. In particular, in Table 2 it is possible to analyze all optimized geometrical configurations each one indicated with the abbreviation "*Type-letter*" referring to Fig. 5, in order to simplify the notation.

From Table 2, it is possible to note that all slot waveguides optimized at 3.39 μm are slightly greater than those optimized at the lower wavelength λ = 2.883 μm. This difference is due to the fact that the longer the operative wavelength, the greater the spatial distribution of the E_x-Field in the guided region.

Table 2. Optimized slot waveguides designed at λ_1 = 3.39 μm and λ_2 = 2.883 μm.

	***w* [nm]**		***h* [nm]**		***g* [nm]**		***t* [nm]**		***s* [nm]**		$S_{h,MAX}$	
Slot waveguide	λ_1	λ_2	λ_1	λ_2	λ_1	λ_2	λ_1	λ_2	λ_1	λ_2	λ_1	λ_2
Type a	410	350	660	530	60	50	40	40	0	0	1.096	1.076
Type b	400	370	690	570	60	60	0	0	0	0	1.081	1.020
Type c	400	360	680	550	60	50	50	40	0	0	1.095	1.047
Type d	400	360	710	570	60	50	0	0	0	0	1.093	1.042
Type e	400	360	690	550	60	50	30	30	0	0	1.097	1.048
Type f	380	290	520	480	50	50	20	20	50	50	1.156	1.150
Type g	390	340	560	450	50	50	20	20	50	50	1.156	1.128

In Figs. 6-8, parametric investigations of sensitivity S_h, cover field confinement Γ_c and slot field confinement Γ_s are shown as a function of the slot gap *g*, for each optimized slot waveguide sketched in Fig. 5. In particular, all following plots graphically represent the last iterative procedure of the whole optimization process. In fact, the only parametric geometrical variable considered in the following graphs is the slot gap *g*, because all other dimensions (*t*, *h*, *w, s*) have been already optimized by the iterative approach described above.

Interesting results have been obtained about sensing performances. In fact, in all waveguide configurations at both mid-IR wavelengths, sensitivities can be better than 1 (see Table 2). This means that an effective index change $\Delta n_{eff} > \Delta n_c$ is induced by a cover index shift Δn_c. Although highest sensitivities require a minimum slot gap as $g \sim$ 50-60 nm in all configurations, some practical

considerations can be derived. In fact, g = 50 nm is a very small slot gap, very difficult to be achieved by standard lithographic techniques. However, it is possible to see in Fig. 6 how slot gap values near 100 nm can still assure high sensitivities ($S_h \sim 1$), in all considered slot waveguides.

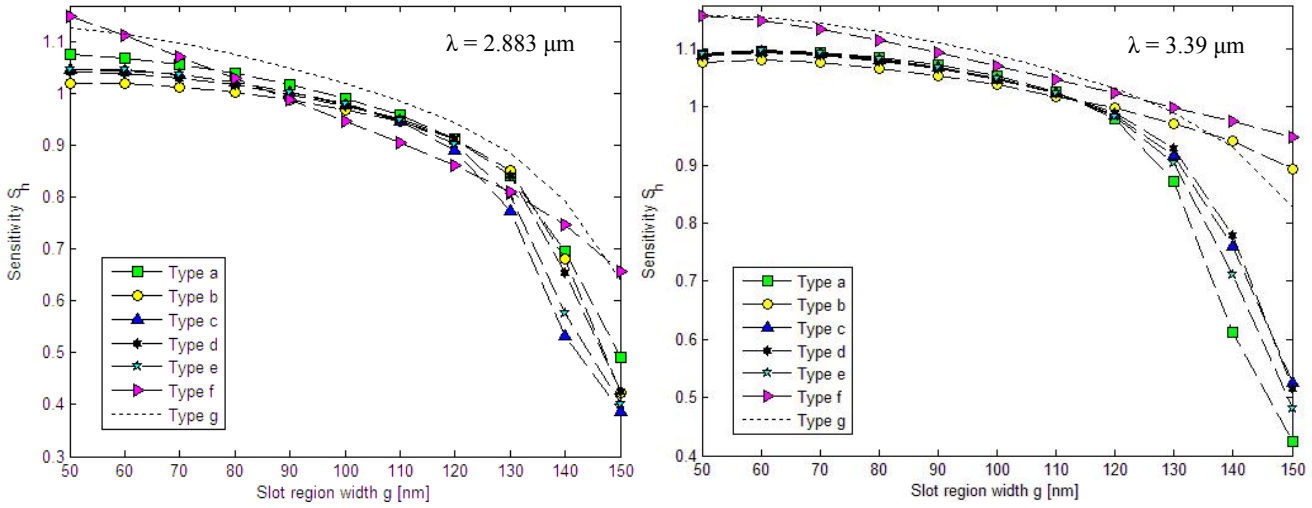

Fig. 6. Sensitivity as a function of slot gap g for optimized slot waveguides with different compositions of group IV materials, at 2.883 μm and 3.39 μm.

Moreover, optimized architectures designed at 3.39 μm exhibits better performances because $S_h > 0.9$, even for g = 120 nm. For slot gap values greater than ~ 100-120 nm, sensitivities significantly decrease because of the low field confinements in cover and slot regions, as shown in Fig. 7.

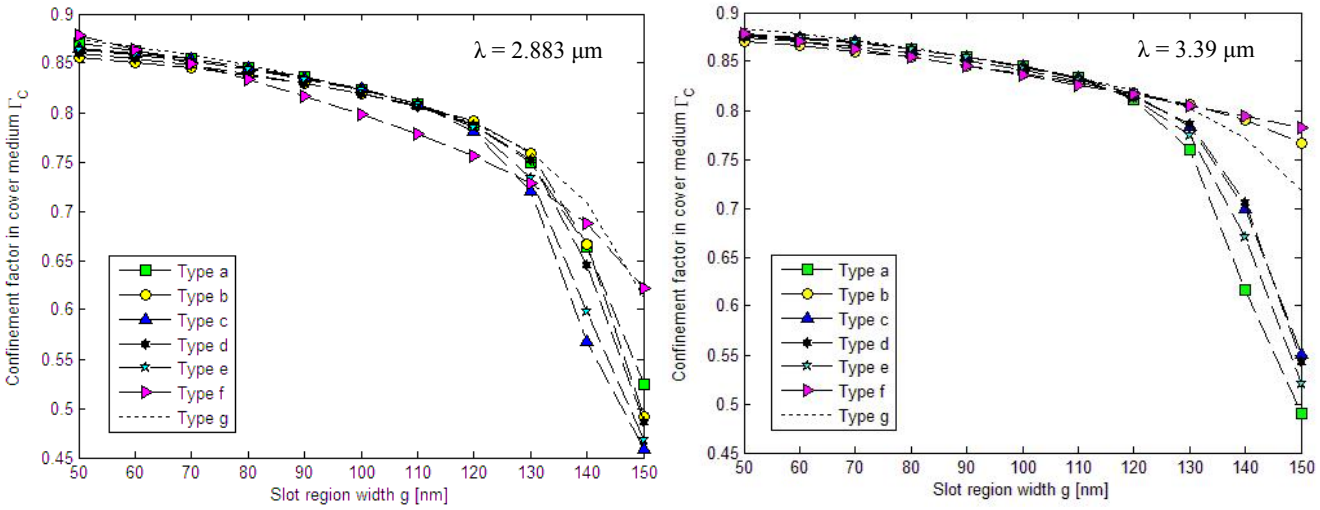

Fig. 7. Cover E_x-field confinement as a function of slot gap g for optimized slot waveguides with different compositions of group IV materials, at 2.883 μm and 3.39 μm.

In Fig. 8, confinement factors in slot region have been plotted for all slot waveguides, as a function of the slot gap g. In particular, it is possible to observe that a great percentage of the optical slot-mode is confined in the slot region, being this one a sub-domain of the whole cover region.

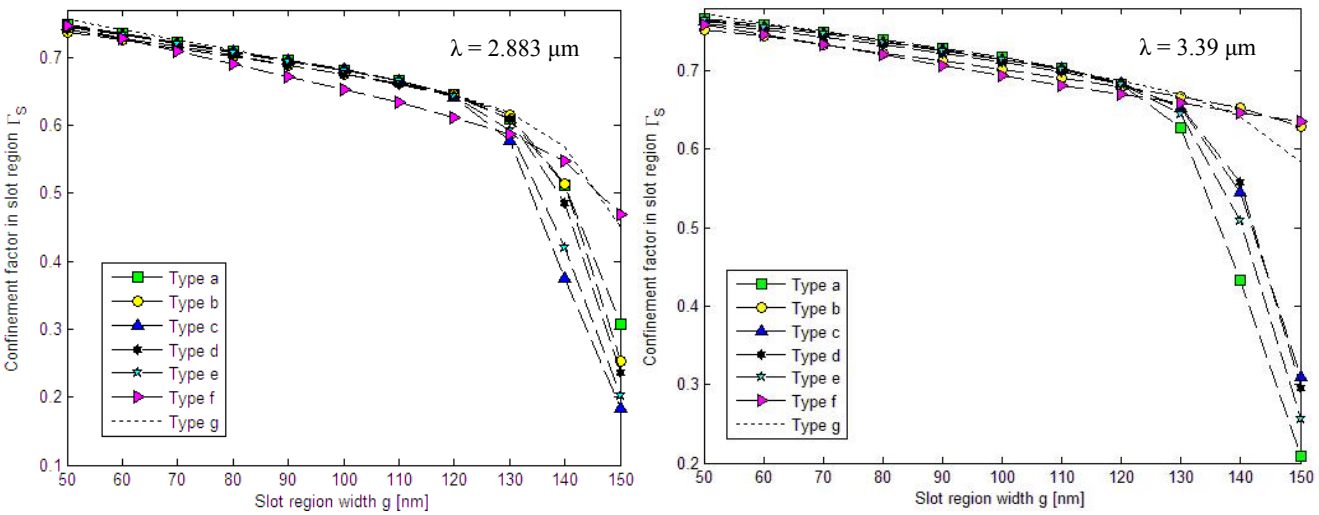

Fig. 8. Slot E_x-field confinement as a function of slot gap g for optimized slot waveguides with different compositions of group IV materials, at 2.883 μm and 3.39 μm.

Important considerations concerning with the analysis of Figs. 6-8, can be carried out. In particular, slot waveguides labeled as "*Type b*", "*Type f*" and "*Type g*" exhibit interesting performance at 3.39 μm. In fact, sensitivities and consequently confinement factors in cover medium and slot region, still remain high ($S_h \sim 0.9$, $\Gamma_c \sim 0.8$, $\Gamma_s \sim 0.65$) for slot gap $g > 140$ nm. This represents a very interesting property that can certainly relax the fabrication tolerances. In addition, it is possible to observe how sensitivities and confinement factors for homogeneous sensing are all characterized by similar analytical trends. In fact, S_h proportionally depends on Γ_c, according to Eq. (4).

In Fig. 9, it is possible to see the characteristic trend affecting effective indices in each investigated SOI-based waveguide configuration. The following plots can be considered as mode-propagation maps, enabling to predict the slot waveguide modal behavior.

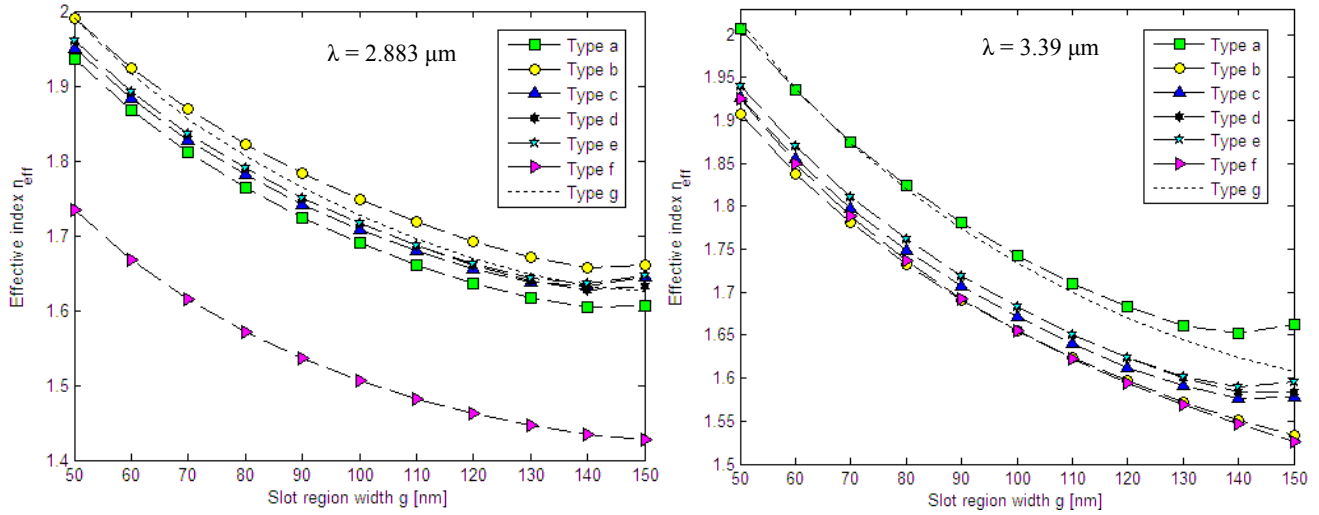

Fig. 9. Waveguide TE effective indices as a function of slot gap g, at 2.883 μm and 3.39 μm.

In particular, at both operative wavelengths, effective indices monolithically decrease by enlarging the slot gap from the initial value of 50 nm. In fact, the larger the slot gap, the greater the E_x-field spatial distribution confined in the low index region (slot region). However, an increase of the effective index

trend is evident for a slot gap g > 140 nm for some slot waveguides optimized at 2.883 μm and 3.39 μm (see Fig. 9). This feature can be explained since the slot fundamental mode is no longer guided when g > 140 nm. Thus, the operative range for the geometrical parameter g is extended from 50 nm to 140 nm, for the design of SOI-based slot waveguides.

In conclusion, theoretical investigation presented in this section reveals how the best material combination for mid-IR photonic sensing is characterized by $Si_{0.08}Ge_{0.78}Sn_{0.14}$-on-$Ge_{0.97}C_{0.03}$-on-Si material system. In fact, this slot waveguide exhibits higher sensitivity for a wide range of g values, with respect to other configurations, although their performances are not very different.

4. Fabrication Tolerances and Second Order TE-Polarized Slot Modes

All waveguide configurations shown in Fig. 5, represent an ideal approximation of realistic photonic slot devices. In fact, ideally vertical sidewalls are very difficult to fabricate by etching e.g., inductively coupled plasma (ICP), especially for high aspect ratio structures. Thus, it is needed to analyze the fabrication tolerances in order to complete the theoretical approach used for the design and optimization of slot waveguides. In particular, it is needed to distinguish between already analyzed ideal SOI slot waveguide structures with vertical sidewalls (θ = 0°) and realistic ones, with non-vertical sidewalls ($\theta \neq 0°$), as sketched in Fig. 10.

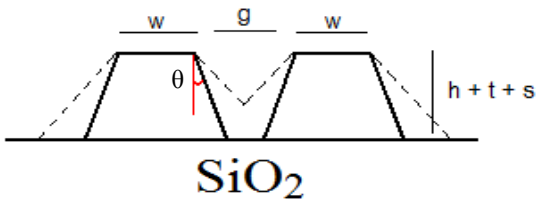

Fig. 10. Schematic representation of fabrication tolerances for SOI-based slot waveguides.

To this purpose, we have considered optimized slot waveguides described in the last paragraph using a different slot gap, i.e. g = 100 nm instead of 50 nm. Thus, same parameters with different values of angle θ, in the range from 0° (vertical sidewalls) to 10° (non-vertical sidewalls), have been evaluated. Results are sketched in Fig. 11 in terms of sensitivity versus tilting angle θ. By observing Fig. 11, it is evident that the greater the tilting angle θ, the smaller the sensitivity. In particular, the maximum tolerance is identified by the angle θ = 4° for all analyzed SOI slot waveguides. In fact, homogeneous sensitivities significantly decrease for tilting angles θ > 4°. Moreover, the slot waveguide "*Type f*" is the best configuration in terms of fabrication tolerances.

In particular, by increasing the tilting angle θ, the E_x-field spatial distribution in the low index region significantly decreases because of the smaller area of the slot region. Consequently, all performance parameters, i.e. S_h, Γ_c, and Γ_s, will be strongly decreased (see Fig. 11). In summary, the geometrical parameter θ can be considered another dimension to be included in the multi-dimensional geometrical space, as in Eq. (8), optimized by implementing the previous iterative method.

4.1. Second Order TE-Polarized Slot Modes

An important property of the optimized slot waveguides, investigated in this paper, is the presence of a second order TE-polarized slot mode-propagation, as plotted in Fig. 12. This property is due to the large dimensions of slot waveguides designed at mid-IR wavelengths. Consequently, it is possible to

select optimized slot structures as multimodal guided-wave structures. Analytical trends of homogeneous sensitivity are quite different with respect to those that have been already obtained for TE slot fundamental mode.

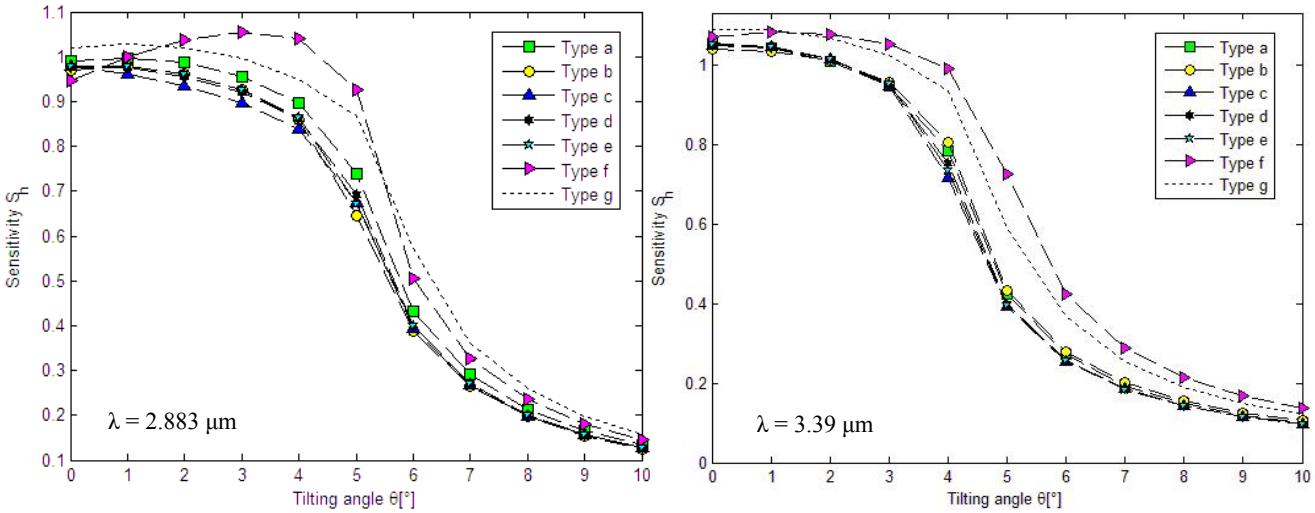

Fig. 11. Sensitivity as a function of the tilting angle θ for different slot waveguide structures, simulated at 2.883 μm and 3.39 μm.

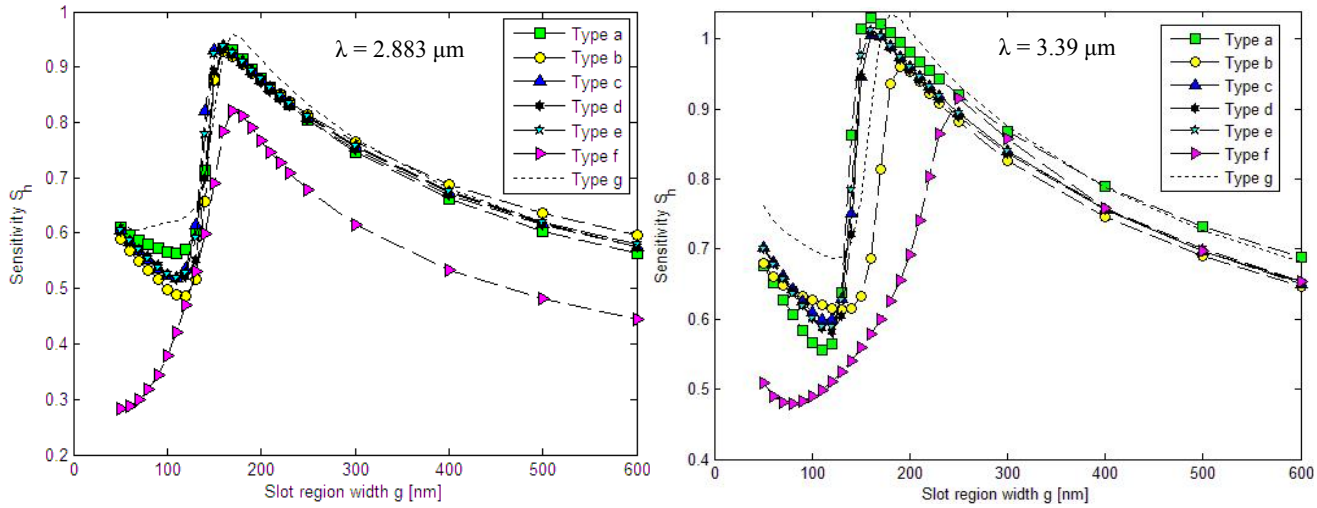

Fig. 12. Homogeneous sensitivities calculated for the second order TE slot modes, propagating in SOI-based slot waveguides, optimized at 2.883 μm and 3.39 μm.

In particular, it is possible to recognize a maximum peak corresponding to the best sensitivities for the same optimized slot waveguide structures as before, with g in the range 160-170 nm, as shown in Fig. 12. In addition, slot waveguides based on $Si_{0.08}Ge_{0.78}Sn_{0.14}$-on-$Ge_{0.91}Sn_{0.09}$-on-Si material system ("*Type f*"), representing one of the best configurations for the fundamental slot-mode propagation as previously analyzed, are the worst in this case. In fact, they exhibit the lowest sensitivity at both operative wavelengths, as compared to all other slot configurations.

In conclusion, the principal advantage induced by the propagation of the second order TE-polarized slot mode at both mid-IR operative wavelengths, consists in the possibility to relax the fabrication tolerances. In fact, high performance (S_h ~ 1) can be achieved with larger slot region gaps

(g ~ 160-200 nm), with respect to g values around 50-60 nm, previously obtained for fundamental mode (see Fig. 6).

5. Comparison between Standard SOI-Based Slot Waveguides Optimized at 1.55 µm, 2.883 µm and 3.39 µm

An interesting comparison between standard SOI slot waveguides (see Figs. 1-2) has been performed, by considering all optimized structures with highest sensitivity at 3.39 µm, 2.883 µm and 1.55 µm telecommunication wavelength. In Table 3 geometrical variables of optimized standard SOI slot waveguides are listed for each operative wavelength considered in our simulations. In particular, it is possible to observe that the longer the wavelength, the greater the waveguide sizes according to similar investigations already done about optimized slot waveguides based on group IV material systems (see Table 2).

Table 3. Optimized standard SOI slot waveguides designed at 1.55 µm, 2.883 µm and 3.39 µm.

Wavelength [nm]	w [nm]	h [nm]	g [nm]	$S_{h,MAX}$
1550	230	500	50	0.880
2883	450	650	80	0.831
3390	520	800	100	0.866

In Fig. 13, sensitivities (S_h) can be observed for a comparison between different slot structures.

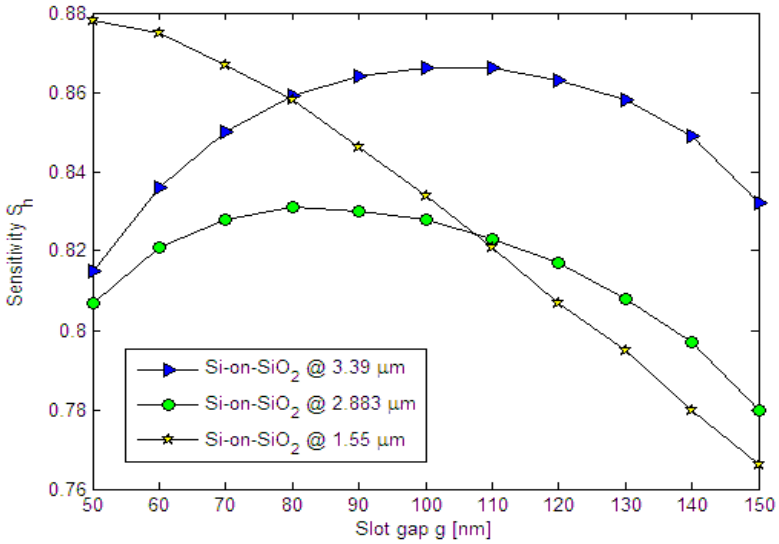

Fig. 13. Sensitivity as a function of slot gap g calculated for optimized SOI slot waveguides, designed and simulated at 1.55 µm, 2.883 µm and 3.39 µm.

Moreover, analogous investigations about confinement factors Γ_c, and Γ_s have been carried out, as shown in Fig. 14. Standard slot waveguides, as analyzed above, exhibit acceptable performance for homogeneous sensing (S_h ~ 0.8-0.9) at each operative wavelength, as considered in the theoretical investigation.

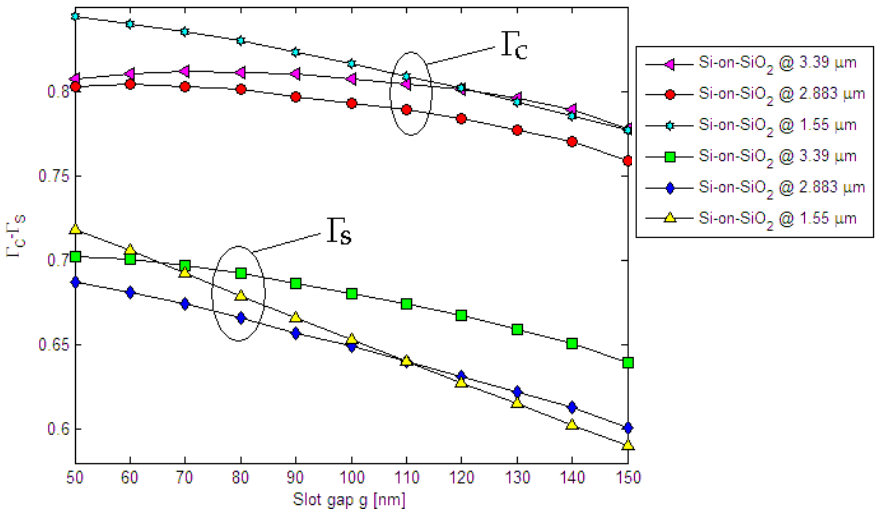

Fig. 14. Confinement factors Γ_c, and Γ_s as a function of the slot gap g calculated for optimized SOI slot waveguides, designed and simulated at 1.55 μm, 2.883 μm and 3.39 μm.

However these performances and, in particular, the sensitivities are lower than those obtained using the novel slot structures based on group IV alloys, as proposed in this paper (S_h > 1). In addition, numerical results demonstrate that standard SOI slot waveguides are characterized by lower fabrication tolerances with respect to novel slot waveguides based on group IV material systems. In fact, in Fig. 15 (left) it is possible to observe that, for tilting angles θ > 2°, sensitivities quickly decrease to unacceptable values for sensing applications, at each of three operative wavelengths.

By this way, the immediate solution to the problem of fabrication tolerances, could include the etching process optimization for the fabrication of slot-based photonic devices. For example, it is possible to improve both selectivity and anisotropy of the process in order to obtain lower tilting angles and, consequently, square-like geometries of slot wires. However, it is important to ensure large tolerance margins for tilting angle in order to simplify the fabrication processes. To this purpose, novel slot waveguides optimized at 3.39 μm and 2.883 μm, satisfy this important design requirement.

The analysis has been completed by the investigation of the second order slot mode propagating in standard slot waveguides presented above. Interesting results have been shown in Fig. 15 (right). In fact, although at both mid-IR operative wavelengths (2.883 μm and 3.39 μm), functional shapes are quite similar and reflect analogous behaviors like those analyzed in previous numerical results (see Fig. 12), optimum sensitivities are the lowest obtained until now. In fact, the standard SOI slot waveguide optimized at 3.39 μm exhibits a sensitivity of 0.856 at g = 190 nm, while that optimized at 2.883 μm is characterized by a sensitivity of 0.79 at g = 200 nm.

Last consideration concerns with the theoretical demonstration of the impossibility to excite the second order TE-polarized slot mode in the standard SOI slot waveguide optimized at the telecommunication wavelength, λ = 1.55 μm. The absence of this modal propagation is justified by the smaller dimensions of this waveguide versus similar structures designed at greater wavelengths (see Table 3).

6. Integrated Ring Resonators for Homogeneous Sensing in Mid-IR

The integration of novel photonic slot waveguides based on group IV material systems in sophisticated photonic architectures, such as ring resonators, is expected to be an efficient readout technique, showing very interesting performance in terms of wavelength shift per refractive index unit (RIU).

This possibility has been also simulated and some values of wavelength sensitivity (WS) $\Delta\lambda/n_c$ and limit of detection (LOD), defined as in Eq. (9), have been calculated for ring resonators based on optimized structures presented in the previous section (see Table 2):

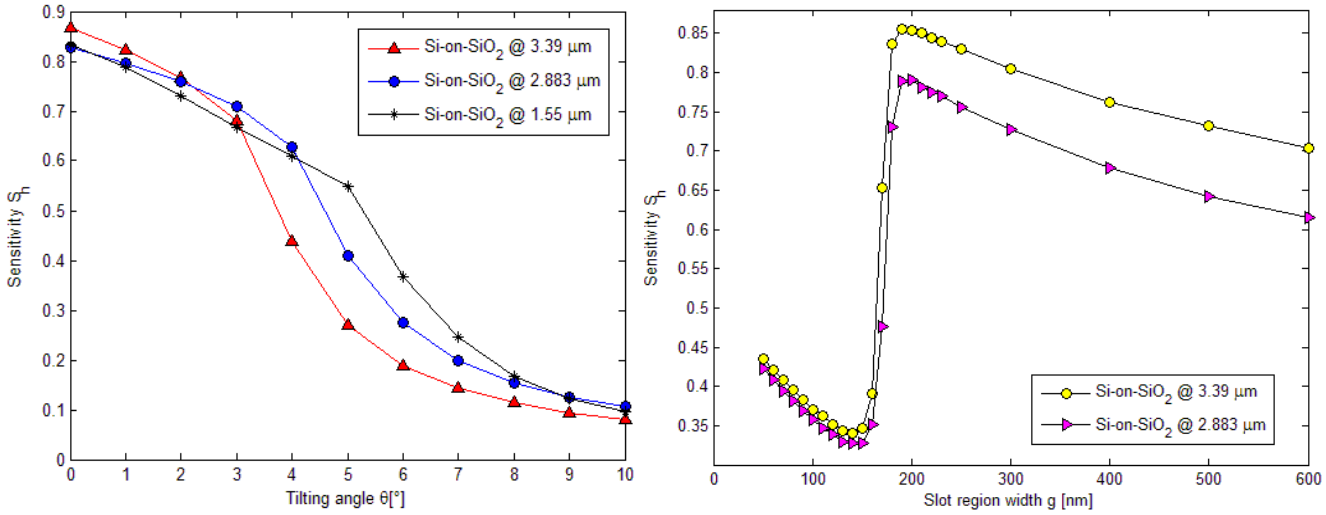

Fig. 15. Sensitivity as a function of the tilting angle θ calculated for optimized SOI slot waveguides, designed and simulated at 1.55 μm, 2.883 μm and 3.39 μm (left). Sensitivity calculated for second order TE slot mode in SOI-based slot waveguides, optimized at 2.883 μm and 3.39 μm (right).

$$WS = S_{slot}\frac{\lambda}{n_{eff\,(air)}}; \quad LOD = \frac{\Delta\lambda}{WS}, \tag{9}$$

where S_{slot} is the homogeneous sensitivity of the optimized slot waveguide considered in previous investigation, λ is the operative wavelength and n_{eff} is the effective index of fundamental TE slot mode that propagates in the slot waveguide covered by air. Consequently, LOD is again defined as the ratio between the wavelength resolution $\Delta\lambda$ and the wavelength sensitivity. In particular, $\Delta\lambda$ as low as 80 pm or less is practical in ordinary optical spectrum analyzers.

In this investigation, slot region gap g has been always set to 100 nm in all optimized slot waveguide configurations, whose geometrical parameters have been listed in Table 2. This choice is justified as a best trade-off between conflicting requirements, i.e. highest sensitivity (requiring g ~ 50-60 nm) and greater size tolerance margins, obtainable with greater slot region gaps.

In Table 4, homogeneous sensitivities and effective indices calculated for optimized slot waveguides characterized by a slot region gap g = 100 nm, have been summarized. Consequently, these values have been implemented for calculation of WS and LOD, according to Eq. (9). To this purpose, it is possible to analyze all performance parameters of ring resonators based on optimized group IV slot waveguides, in Table 5.

Interesting results have been achieved. In particular, a limit of detection as low as 3.64×10^{-5} RIU could be obtained in the slot waveguide labeled as "*Type f*" ($Si_{0.08}Ge_{0.78}Sn_{0.14}$-on-$Ge_{0.91}Sn_{0.09}$-on-Si) optimized at 3.39 μm, exhibiting a wavelength sensitivity WS, as large as 2194 nm/RIU. In summary, it is possible to note that the principal difference in terms of performance parameters of novel slot waveguides, concerns with the mid-IR operative wavelength. In fact, all slot waveguides optimized at 3.39 μm exhibit larger values of WS and LOD, as compared to structures optimized at 2.883 μm.

Table 4. Homogeneous sensitivities of optimized SOI slot waveguides with g = 100 nm.

Optimal structures	S_h		n_{eff}	
	λ_1= 3.39 μm	λ_2 = 2.883 μm	λ_1 = 3.39 μm	λ_2 = 2.883 μm
Type a	1.054	0.991	1.743252	1.690110
Type b	1.038	0.970	1.655458	1.748301
Type c	1.048	0.979	1.670879	1.707916
Type d	1.048	0.977	1.682615	1.716042
Type e	1.050	0.980	1.682845	1.716391
Type f	1.071	0.947	1.655238	1.506740
Type g	1.089	1.021	1.734429	1.727081

Table 5. Performance parameters of ring resonators based on group IV slot waveguides (g = 100 nm), designed for homogeneous sensing in mid-IR.

Optimal structures	WS [nm/RIU]		LOD [RIU]	
	λ_1= 3.39 μm	λ_2 = 2.883 μm	λ_1 = 3.39 μm	λ_2 = 2.883 μm
Type a	2050	1690	3.90×10^{-5}	4.73×10^{-5}
Type b	2126	1600	3.76×10^{-5}	5.00×10^{-5}
Type c	2126	1652	3.76×10^{-5}	4.84×10^{-5}
Type d	2111	1641	3.79×10^{-5}	4.87×10^{-5}
Type e	2115	1646	3.78×10^{-5}	4.86×10^{-5}
Type f	2194	1812	3.64×10^{-5}	4.41×10^{-5}
Type g	2128	1704	3.76×10^{-5}	4.70×10^{-5}

Moreover, a comparison between these photonic structures realized with an appropriate combination of group IV materials and alloys, and some results in literature, both experimental and theoretical, confirm the potential of these novel slot waveguides. In fact, ring resonators based on standard SOI slot waveguides optimized at 1.55 μm for homogeneous sensing in aqueous solution, exhibit WS ~ 1000 nm/RIU and LOD = 8×10^{-5} [8]. Moreover, a ring resonator based on a SOI ridge guiding structure optimized at 1.55 μm for homogeneous sensing of ammonia, is characterized by WS = 140 nm/RIU and LOD = 8×10^{-5} [17]. In conclusion, a gas sensor based on a photonic crystal cavity has been proved to exhibit WS = 80 nm/RIU and LOD = 1×10^{-4} [18]. All data reported above emphasize ultra-high performances that characterize the group IV slot waveguides proposed in this investigation.

6.1. Application: Methane Homogeneous Sensing at 3.39 μm

The main advantage of operating in mid-IR wavelength range, consists in the possibility to reflect the molecularly characteristic arrangement of chemical bonds in several analytes within the probed molecules, via the frequency position of the associated vibrations and mixed rotational-vibrational transitions. In addition, a lot of environmental harmful gases like carbon dioxide (CO_2), methane (CH_4) and ammonia (NH_3), to name a few, are characterized by absorption spectra in mid-IR as previously sketched in Fig. 4.

In this section, an interesting application of a novel ring resonator based on group IV slot waveguide designed and optimized at 3.39 μm, is reported for homogeneous sensing of methane whose absorption spectra is show in Fig. 16. In particular, the slot waveguide selected for this investigation is that labeled as "*Type f*" ($Si_{0.08}Ge_{0.78}Sn_{0.14}$-on-$Ge_{0.91}Sn_{0.09}$-on-Si), because it exhibits the best performance in terms of WS = 2194 nm/RIU and LOD = 3.64×10^{-5} RIU, at the mid-IR operative wavelength λ = 3.39 μm.

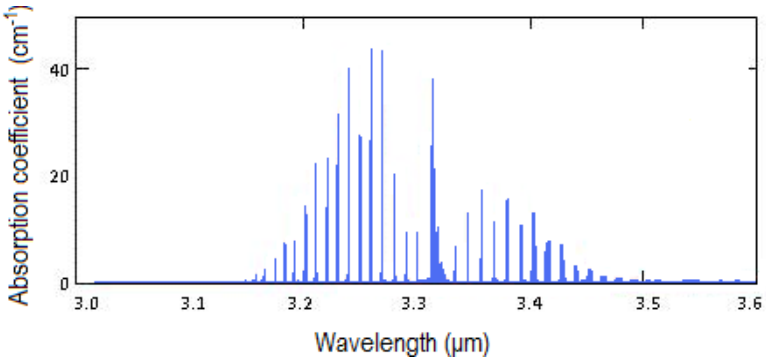

Fig. 16. Methane absorption spectrum in mid-IR.

Numerical results have been obtained by simulating the methane gas sensing in standard conditions for temperature and pressure (T = 0 °C, P = 1 atm). The ring-slot resonator considered in the calculation, is coupled to a bus slot-waveguide as sketched in Fig. 17 (left).

Initially the sensor, in particular the sensible region, is exposed to pure air (100 %) and its transmission spectrum exhibits a resonant peak at 3.39 μm. When the sensor is exposed to a mixture of air (50 %) and methane (50 %), it is possible to register two simultaneous phenomena. In particular, by assuming an effective index change $\Delta n_{eff} \sim 1 \times 10^{-4}$ due to the methane presence in the gas mixture in device cover medium (n_{Air} = 1.000292, n_{CH4} = 1.000444), a wavelength shift $\Delta\lambda \sim 190$ pm of the same resonant peak in the photonic sensor transmission spectra can be observed, as in Fig. 17 (right). This wavelength shift enables the methane detection process to occur through a device wavelength interrogation.

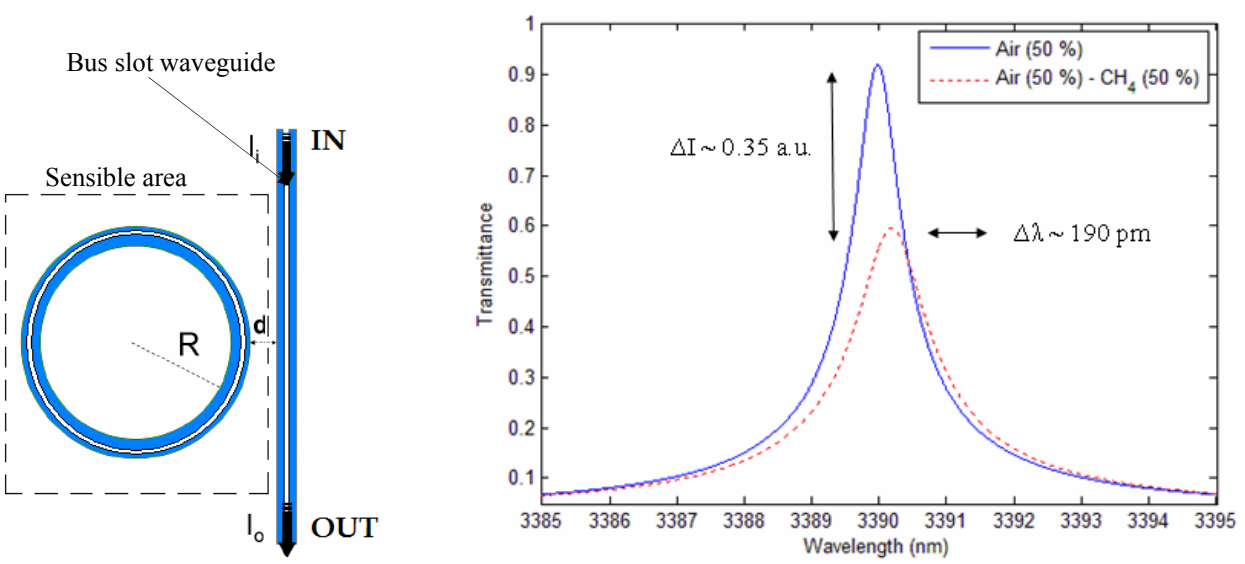

Fig. 17. Ring resonator based on group IV slot waveguide (*Type f*) optimized at λ = 3.39 μm, with a ring radius R = 63 μm (left). Both wavelength and power interrogation can participate to the sensor readout (right).

Moreover, methane is characterized by an absorption coefficient α_A = 15 cm^{-1} at 3.39 μm. Then, it is possible to define a total propagation loss as follows:

$$\alpha_{TOT} = \alpha_P + \alpha_A \ , \tag{10}$$

where α_P represents the waveguide optical propagation loss set to 1 dB/cm and α_A is a function of the

operative wavelength, according to Fig. 16. Thus, both optical absorption and homogeneous sensing simultaneously occur in our device. In fact, the transmission spectra of the ring-slot sensor is also characterized by an intensity reduction according to Eq. (6). In addition, an interaction length L of about 400 μm ($2\pi R$ for R= 63 μm) produces a transmittance change $\Delta I \sim 0.35$ a. u. (see Fig. 17, on the right).

In conclusion, both wavelength and power interrogation occur together in the detection process and allow to improve the sensor performances. Moreover, these sensors are able to detect very small volumes (~ 1 μm^3) of gas traces in mid-IR (e.g., 10.3 % methane concentration in air). This is an important result because methane lower and upper explosive limits (LEL and UEL, respectively), thus the minimum and maximum concentration of methane needed to support its combustion in air, are 5 % and 15 % percent by volume in air, respectively, at room temperature and atmospheric pressure. Consequently, it is very important to monitor methane concentration ranging from 5 % and 15 % in order to prevent lethal explosion in dangerous work environments. In addition, photonic sensors as proposed in this paper, can be also used for home safety, for example by locating gas detectors in key areas inside the home, preventing CH_4 poisoning and explosions. Finally, theoretical results can be also compared with commercial infrared gas sensors and detectors [19-20].

7. Conclusions

In this paper, intriguing novel photonic sensors based on unconventional group IV alloys and material systems have been investigated. In particular, a systematic method for design and optimization of novel SOI slot waveguides based on group IV material systems has been proposed. Moreover, a multi-dimensional geometrical space has been defined by taking into account all different waveguide geometrical parameters. An iterative method for the dynamic adjustment of all geometrical dimensions (h, w, g, t, s) has been applied, in order to achieve the best performance configurations in terms of ultra-high sensitivity for homogeneous sensing S_h.

Important considerations concerning with propagation losses in mid-IR, and electronic and optical properties of group IV compounds have been treated, too. Appropriate combinations of group IV compounds have been chosen on the basis of their technological compatibility (e.g., the impossibility to selectively grow the GeSn alloy directly on silicon dioxide) and low losses in mid-IR wavelength range. The design of group IV alloys has been performed in order to maximize the refractive index contrast for increasing the optical field confinement in slot region and, at the same time, to assure optical transparence at selected mid-IR operative wavelengths. Interesting properties such as the presence of a second order TE slot mode, have been demonstrated, giving further flexibility in design. In fact, it is possible to relax the fabrication tolerances as well as realizing integrated photonic devices for high-selective detection in mid-IR, representing a novel, promising and attractive field of research.

In conclusion, ring resonators based on optimized group IV slot waveguides presented in this paper, exhibit very interesting performances. In fact, simulations reveal a minimum detectable methane concentration lower than 10 % by volume in air. In addition, optimized slot waveguides for efficient sensing in mid-IR exhibit much higher performance with respect to standard SOI slot devices designed at near-IR (1.55 μm), with an improvement of more than 110 %. Further work on this topic will be devoted to detailed model and design of slot-based ring resonators constituted by several combinations of group IV materials and alloys, with the aim to further improve the performance of photonic sensors in mid-IR and their use in several application fields.

Acknowledgments

This work has been supported by Fondazione della Cassa di Risparmio di Puglia, Bari, Italy.

References

[1]. P. Bienstman, K. De Vos, T. Claes, P. Debackere, R. Baets, J. Girones and E. Schacht, Biosensors in Silicon on Insulator, *Proc. of the SPIE Silicon Photonics IV*, Vol. 7220, 2009.
[2]. D. M. Sonnenfroh, W. T. Rawlins, M. G. Allen, C. Gmachl, F. Capasso, A. L. Hutchinson, D. L. Sivco, J. N. Baillargeon and A. Y. Cho, Application of balanced detection to absorption measurements of trace gases with room-temperature, quasi-cw quantum-cascade lasers, *Appl. Opt*., Vol. 40, 2001, pp. 812-820.
[3]. Y. Zhang, Wu Gao, Z. Song, Y. An, L. Li, Z. Song, W. W. Yu and Y. Wang, Design of a novel gas sensor structure based on mid-infrared absorption spectrum, *Sensors and Actuators B,* Vol. 147, 2010, pp. 5-9.
[4]. J. T. Robinson, L. Chen and M. Lipson, On-chip gas detection in silicon optical microcavities, *Opt. Express*, Vol. 16, 2008, pp. 4296-4301.
[5]. L. W. Kornaszewski, N. Gayraud, J. M. Stone, W. N. Macpherson, A. K. George, J. C. Knight, D. P. Hand and D. T. Reid, Mid-infrared methane detection in a photonic bandgap fiber using a broadband optical parametric oscillator, *Opt. Express*, Vol. 15, 2007, pp. 11219-11224.
[6]. Comsol Multiphysics by COMSOL, Stockholm, ver. 3.2, 2005, single license.
[7]. M. Iqbal, Z. Zheng, and J. Liu, Light confinement in low contrast slot waveguide structures investigated, in *Proceedings of the ICMMT,* 2008, pp. 878-881.
[8]. F. Dell'Olio and V. M. N. Passaro, Optical sensing by optimized silicon slot waveguides, *Opt. Express*, Vol. 15, 2007, pp. 4977-4993.
[9]. F. De Leonardis, G. Giannoccaro, B. Troia, V. M. N. Passaro and A. G. Perri, Design of Optimized SOI Slot Waveguides for Homogeneous Optical Sensing in Near Infrared, in *Proceedings of the 4th IEEE Int. Workshop on Sensors and Interfaces (IWASI' 2011)*, Savelletri, Italy, 28-29 June 2011.
[10]. V. M. N. Passaro, B. Troia and F. De Leonardis, Group IV Photonic Slot Structures for Highly Efficient Gas Sensing in mid-IR, *Proceedings of the 2nd Int. Conf. on Sensor Dev. Technol. and Applications (SENSORDEVICES' 2011)*, S. Laurent du Var/Nice, France, 21-27 August 2011, pp. 103-108.
[11]. S. Kasap and P. Caper, Handbook of Electronic and Photonic Materials, *Springer Science + Business Media Inc.,* 2006.
[12]. M. Bass, C. De Cusatis and J. Enoch, Handbook of Optics: Optical Properties of Materials, nonlinear optics, quantum optics, 3rd Edition 2009, Vol. 4, *McGraw-Hill*.
[13]. G. Ghosh, Dispersion-equation coefficients for the refractive index and birefringence of calcite and quartz crystal, *Opt. Commun*., Vol. 163, No. 1-3, 1999, pp. 95-102.
[14]. B. Troia, V. M. N. Passaro and F. De Leonardis, Bandgap Engineering and Optical Properties of Group IV Material Compounds, in *Proceedings. Of the 13° National Conf. of Photonic Technologies (Fotonica 2011)*, Genova, 9-11 May 2011.
[15]. R. Soref, S. J Emelett and W. R. Buchwald, Silicon waveguided components for the long-wave infrared region, *J. Opt. A: Pure Appl. Opt.,* Vol. 8, 2006, pp. 840-848.
[16]. Guo-En Chang, S.-W. Chang and S. L. Chuang, Strain-Balanced Ge_zSn_{1-z} - $Si_xGe_ySn_{1-x-y}$ Multiple-Quantum-Well Lasers, *IEEE J. Quantum Electron*., Vol. 46, 2010, pp. 1818-1820.
[17]. V. M. N. Passaro, F. Dell'Olio and F. De Leonardis, Ammonia Optical Sensing by Microring Resonators, *Sensors,* Vol. 7, No. 11, 2007, pp. 2741-2749.
[18]. T. Sunner, T. Stichel S. -H. Kwon, T. W. Schlereth, S. Holfing, M. Kamp and A. Forchel, Photonic crystal cavity based gas sensor, *Appl. Phys. Lett*., Vol. 92, No. 26, 2008, art. 261112.
[19]. http://www.net-safety.com
[20]. http://www.gassensor.com.cn

Sensors & Transducers Journal

Guide for Contributors

Aims and Scope

Sensors & Transducers Journal (ISSN 1726-5479) provides an advanced forum for the science and technology of physical, chemical sensors and biosensors. It publishes state-of-the-art reviews, regular research and application specific papers, short notes, letters to Editor and sensors related books reviews as well as academic, practical and commercial information of interest to its readership. Because of it is a peer reviewed international journal, papers rapidly published in *Sensors & Transducers Journal* will receive a very high publicity. The journal is published monthly as twelve issues per year by International Frequency Sensor Association (IFSA). In additional, some special sponsored and conference issues published annually. *Sensors & Transducers Journal* is indexed and abstracted very quickly by Chemical Abstracts, IndexCopernicus Journals Master List, Open J-Gate, Google Scholar, etc. Since 2011 the journal is covered and indexed (including a Scopus, Embase, Engineering Village and Reaxys) in Elsevier products.

Topics Covered

Contributions are invited on all aspects of research, development and application of the science and technology of sensors, transducers and sensor instrumentations. Topics include, but are not restricted to:

- Physical, chemical and biosensors;
- Digital, frequency, period, duty-cycle, time interval, PWM, pulse number output sensors and transducers;
- Theory, principles, effects, design, standardization and modeling;
- Smart sensors and systems;
- Sensor instrumentation;
- Virtual instruments;
- Sensors interfaces, buses and networks;
- Signal processing;
- Frequency (period, duty-cycle)-to-digital converters, ADC;
- Technologies and materials;
- Nanosensors;
- Microsystems;
- Applications.

Submission of papers

Articles should be written in English. Authors are invited to submit by e-mail editor@sensorsportal.com 8-14 pages article (including abstract, illustrations (color or grayscale), photos and references) in both: MS Word (doc) and Acrobat (pdf) formats. Detailed preparation instructions, paper example and template of manuscript are available from the journal's webpage: http://www.sensorsportal.com/HTML/DIGEST/Submition.htm Authors must follow the instructions strictly when submitting their manuscripts.

Advertising Information

Advertising orders and enquires may be sent to sales@sensorsportal.com Please download also our media kit: http://www.sensorsportal.com/DOWNLOADS/Media_Kit_2012.pdf